Reference Governor for Load Control in a Multicylinder Recompression HCCI Engine

Shyam Jade, *Student Member, IEEE*, Erik Hellström, *Member, IEEE*, Jacob Larimore, *Student Member, IEEE*, Anna G. Stefanopoulou, *Fellow, IEEE*, and Li Jiang

***Abstract*— This paper presents a model-based control strategy designed to regulate combustion phasing during load transitions in a recompression homogeneous charge compression ignition (HCCI) engine. A low-order discrete-time control-oriented model for recompression HCCI combustion is developed that represents the strong thermal and composition coupling between engine cycles. A baseline two-input single-output controller is designed to regulate combustion phasing, using the amount of negative valve overlap and the fuel injection timing as actuators. This controller is augmented by a reference or fuel governor, which modifies transient fuel mass commands during large load transitions, when future actuator constraint violations are predicted. This approach is shown in experiments to improve combustion phasing and load responses, preventing engine misfires in some cases. The fuel governor enables larger load transitions than were possible with the baseline controller alone. The governor acts only when future actuator constraint violations are predicted. The complexity and computational overhead of the governor are reduced by developing a linearized fuel governor. Satisfactory performance is demonstrated experimentally for a range of engine speeds.**

***Index Terms*— Homogeneous charge compression ignition (HCCI) combustion, internal combustion engines, nonlinear dynamical systems, powertrain control, predictive control, reference governor.**

I. Introduction

HOMOGENEOUS charge compression ignition (HCCI) is a promising low-temperature combustion strategy that combines high thermal efficiency with low engine-out emissions. It is characterized by near simultaneous compression-driven autoignition events at multiple sites throughout a uniformly mixed air–fuel mixture, see [1], [2]. HCCI combustion control poses challenges that must be overcome before it can be commercially implemented. This paper presents a model-based control strategy for the regulation of combustion phasing during load transitions in a gasoline recompression HCCI engine.

Autoignition timing control in HCCI combustion requires careful regulation of the temperature, pressure, and composition of the precombustion cylinder charge. The combustion phasing or timing is constrained within a narrow acceptable range [3], [4]. Early combustion causes excessive pressure rise rates that violate noise and mechanically stress constraints. Late phasing leads to incomplete combustion and significant amounts of unburned fuel being retained between cycles. This can cause unacceptably high cyclic variability (CV) and torque fluctuations.

The transient response during load transitions in HCCI engines can violate the acceptable combustion phasing range, even if the steady-state operating points lie within this range. Load transitions are primarily achieved through fuel mass changes, which have a significant effect on charge temperature and consequently on combustion phasing. Combustion phasing regulation during large transients can lead to actuator saturation, and a subsequent loss in controller authority and regulation performance. This is most pronounced during load steps down, when the reduced charge temperatures can cause excessively late combustion phasing and engine misfires. Misfires are unacceptable for emissions and driveability.

Solutions to this problem using optimal control have been proposed, see for example [5]–[7]. However, these involve the on-line solving of a nonlinear optimization problem where the stabilization, tracking, and actuator constraint requirements have to be satisfied simultaneously. This problem is simplified using the current strategy, which reduces computation time compared with higher-dimensional optimal control schemes, at the cost of reduced flexibility in shaping the transient response.

The methodology proposed is outlined in Fig. 1. Load requirements are converted into desired fuel mass commands (m_f^{des}). A baseline controller uses valve and fuel injection timings to track desired combustion phasing ($\theta_{50}^{\mathrm{ref}}$). The fuel governor is then added on to the controller-augmented nonlinear system to improve load transition responses. It works by attenuating the desired fuel amount change when future actuator constraint violations are predicted, see [8], [9].

The fuel governor is based on the reference governor concept that separates closed loop design from the constraint enforcement requirement [10]–[14]. Reference governors can be defined as nonlinear devices which are added to a primal compensated linear system to modify, when necessary, the reference signal in such a way the constraints are enforced

Manuscript received January 4, 2013; revised June 27, 2013; accepted September 8, 2013. Manuscript received in final form September 22, 2013. Date of publication October 16, 2013; date of current version June 16, 2014. This work was supported in part by the Department of Energy, in part by the National Energy Technology Laboratory under Award DE-EE0003533, in part by the ACCESS project consortium with direction from Hakan Yilmaz and Oliver Miersch-Wiemers, and in part by Robert Bosch, LLC. Recommended by Associate Editor S. Di Cairano.

S. Jade, E. Hellström, J. Larimore, and A. G. Stefanopoulou are with the Department of Mechanical Engineering, University of Michigan, Ann Arbor, MI 48109 USA (e-mail: sjade@umich.edu; erikhe@umich.edu; larimore@umich.edu; annastef@umich.edu).

L. Jiang is with Robert Bosch LLC, Farmington Hills, MI 48331 USA (e-mail: li.jiang@us.bosch.com).

Color versions of one or more of the figures in this paper are available online at http://ieeexplore.ieee.org.

Digital Object Identifier 10.1109/TCST.2013.2283275

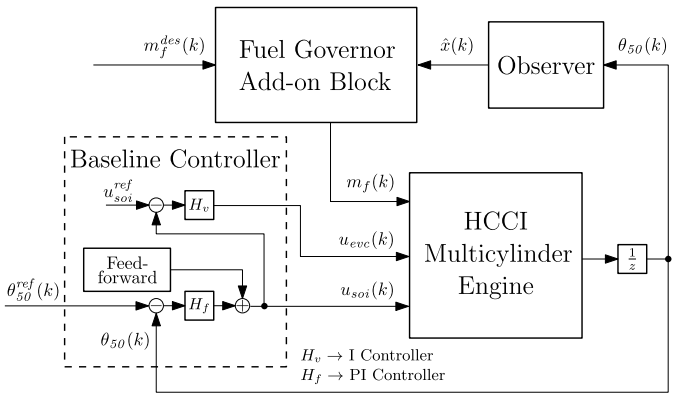

Fig. 1. System overview: The fuel governor is added on to the controller-augmented system. Estimated states are obtained from the observer.

and the compensated system maintains its linear behavior [13]. Reference governors have been applied widely, for example, to prevent fuel cell oxygen starvation [15]–[17], in hydroelectric power generation [18], [19] and in turbocharged diesel engine supplemental torque control [20].

The authors first introduce the fuel governor methodology as a solution for the HCCI load transient control problem in [8]. These simulation results are augmented with preliminary experimental validation results in [9]. This paper builds on these two publications. The range of validity of the HCCI control-oriented model is extended to engine speeds other than the nominal 1800 r/min. This enables the development of a globally valid fuel governor controller without the need for speed-based gain scheduling and multiple model linearizations, as proposed in [9]. New experimental results are presented for different engine speeds.

This paper is structured as follows. The multicylinder recompression HCCI engine and control hardware are introduced in Sections II and III. A control-oriented model for HCCI combustion is presented in Section IV, along with steady-state and transient validation results in Section V. The model is used in Section VI to develop a baseline controller that tracks combustion phasing. The phasing and load-tracking performance during large load transitions is improved by implementing the fuel governor in Section VII. The governor enables larger load transitions than were possible with the baseline controller alone. The linearized fuel governor is developed to reduce computational complexity with a minor loss in performance. Validation at different engine speeds is presented.

II. Experimental Setup

A turbocharged, direct-injection, inline four-cylinder GM LNF Ecotec engine with an engine displacement of 2.0 L was used in this paper, see Table I. Premium grade indolene fuel was used for all experiments. Modifications to the engine for HCCI combustion included an increased geometric compression ratio of 11.25:1, and shorter duration and lower lift cam profiles to allow for unthrottled operation. In addition to the stock turbo charger, an Eaton M24 supercharger was used to boost intake manifold pressure. Most of the results presented in this paper were run at slightly boosted conditions,

TABLE I
Experimental Engine Geometry

Parameter	Value	Parameter	Value
Displacement	2.0 L	Bore	86 mm
Number of cylinders	4	Stroke	86 mm
Compression ratio	11.25	Connecting rod length	145.5 mm
Wrist Pin Offset	0.8 mm		

approximately 1.1 bar intake manifold pressure. The relative air–fuel ratio λ varied between $1 \rightarrow 1.3$. Engine coolant temperature was controlled to a set-point of 90 °C for all tests. The spark was left on to prevent fouling, but was fixed at 40 °CA after top dead center (aTDC) to prevent interference with HCCI combustion.

In-cylinder pressure was sampled at a resolution of 0.1 °CA for offline pressure trace analysis, and at a resolution of 1 °CA for real-time estimation of combustion features. The offline analysis tool estimates the mass fraction burned curve, the work output, the in-cylinder temperature trace, the residual gas fraction, and the cylinder mass flows. Details of the offline heat release analysis method can be found in [3], [21], and [22]. Combustion phasing θ_{50} used in feedback control was estimated using the built-in functionality of the Bosch Motronic MED17 engine control unit (ECU). The θ_{50} and indicated mean effective pressure (IMEP) predictions from the ECU were validated with values obtained from offline pressure trace analysis, and they differ only by fixed offsets.

The control strategies were implemented using C and MATLAB code, and were tested in real-time using an ETAS ES910 rapid prototyping module. The module uses an 800-MHz Freescale PowerQUICC III MPC8548 processor with double-precision floating point arithmetic and 512 MB of RAM.

III. Recompression HCCI

Autoignition in HCCI combustion is a thermally driven chemical kinetic process [1], [23]. To phase autoignition around TDC, the temperature of the precombustion charge has to be significantly higher than that typically seen in conventional spark ignition (SI) combustion at the same engine load-speed operating point. The actuation strategy chosen to achieve this is recompression, which is an efficient and relatively quick strategy for affecting charge temperature [24], [25].

In recompression HCCI the exhaust valve is closed early and the intake valve is opened late, compared with typical SI operation [24]. The resulting negative valve overlap (NVO) can be seen in the typical recompression HCCI in-cylinder pressure trace of Fig. 2. A large fraction of the in-cylinder charge is trapped before it can be exhausted. These trapped gases set up strong thermal and composition coupling between engine cycles.

A. Control Actuators

The actuator inputs considered for control are a single value of the exhaust valve closing timing (u_{evc}), four values of the

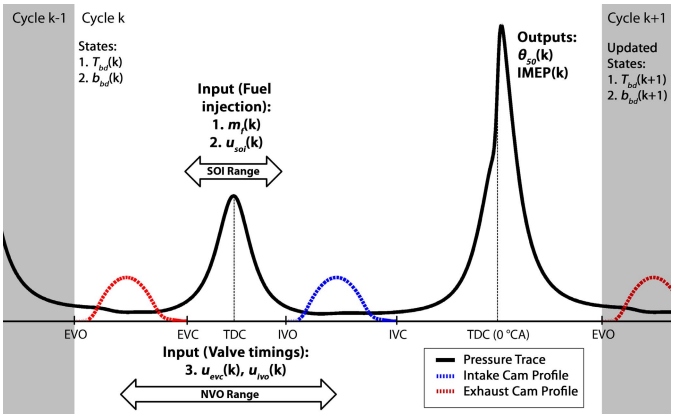

Fig. 2. Typical recompression HCCI pressure trace, showing the relative locations of inputs, outputs, and states. The recompression pressure rise caused by the NVO can be clearly seen.

start of fuel injection timing (u_{soi}), and four values of the mass of fuel injected (m_f^{inj}). Environmental conditions such as the pressure and temperature of the manifolds affect combustion, but these are not controlled.

1) Exhaust Valve Closing Timing: Manipulating u_{evc} changes the mass fraction of hot residuals trapped in the cylinder, which significantly affects the coupling between engine cycles. Valve timings are controlled by a hydraulic cam phasing actuator that phases (moves) the intake or exhaust cams of all cylinders simultaneously. Thus, the cam phasing actuator cannot be used for cylinder-individual control. The cam profiles are fixed, which means that the valve opening and closing timings cannot be changed independently. In this paper, the exhaust cam position is varied, while the intake cam position is fixed. The cam phasing actuator is slow and is subject to a rate constraint.

2) Start of Fuel Injection Timing: Fuel injection timing is recognized in literature as an important part of the control strategy for recompression HCCI engines [24], [26], [27]. As seen in Fig. 2, the fuel amount is injected in a single injection, the timing of which can be varied within the recompression region. The start of fuel injection timing (u_{soi}) can be set independently for each cylinder, and is thus useful for cylinder-to-cylinder combustion phasing balancing. It can also be set independently from cycle-to-cycle, which makes u_{soi} a fast actuator with no rate constraints.

Injecting fuel into the hot residual gases has complex thermal and chemical effects [26], the net effect of which is that earlier injection leads to earlier autoignition. Varying u_{soi} does not have a large effect on the engine load in general. Very early u_{soi} can adversely affect pumping work and emissions [28].

3) Mass of Fuel Injected: In SI engines, the mass of fuel injected (m_f^{inj}) is typically used to maintain high emissions after-treatment efficiency by regulating the air–fuel ratios of the individual cylinders to stoichiometric conditions. Since low-temperature HCCI combustion generates low levels of engine-out NO_x, maintaining stoichiometry is not a concern. The combustion is run at lean conditions to improve fuel economy, and the m_f^{inj} actuator can be used for other purposes.

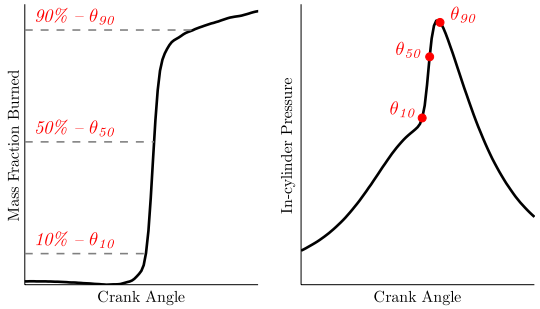

Fig. 3. Engine crank angles where 10%, 50%, and 90% of heat release occur. The mass fraction burned curve (left) is computed offline from the measured in-cylinder pressure trace (right).

The fuel amount is strongly correlated with the work output, IMEP in HCCI combustion, and is hence used to control the desired engine load. The mass of fuel injected can be used for cylinder-to-cylinder load balancing, as m_f^{inj} can be varied independently for each cylinder. Changing m_f^{inj} also has a significant effect on charge temperature, and consequently on combustion phasing. During load transitions, these undesirable changes in combustion phasing need to be compensated for by the other control inputs, namely u_{soi} and u_{evc}. In this paper, m_f^{inj} transients will be shaped to smooth load transitions.

B. Performance Outputs

Combustion phasing or timing is the primary output to be controlled. This is quantified by the location of θ_{50}, which is the engine crank angle at which 50% of the total heat release occurs. This measure is a reliable indicator of the location of combustion [29], [30]. In practice, the mass fraction burned curve is computed through heat release analysis of the in-cylinder pressure traces. It is preferable to use θ_{50} to characterize combustion as its location is relatively insensitive to changes in heat release analysis assumptions. Fig. 3 shows the location of the engine crank angles where 10%, 50%, and 90% of the heat release occur.

The work output, represented by the IMEP, is defined [31] as the total pressure-volume work integrated over an engine cycle, normalized by the displacement volume (V_d)

$$\text{IMEP} = \int p \frac{\mathrm{d}V}{V_d} \tag{1}$$

where p and V are the in-cylinder pressure and volume, respectively. IMEP is seen to be a very strong function of the mass of fuel injected (m_f^{inj}).

IV. Control-Oriented Model

Designing combustion phasing controllers for multicylinder recompression HCCI engines requires control-oriented models that capture all important dynamics, while being simple enough for controller development purposes. This paper builds on [32] and focuses on modeling HCCI combustion for operating regimes with near complete combustion and low cycle-to-cycle variability. In general, it is desired that combustion be maintained in these regions for driveability and fuel economy.

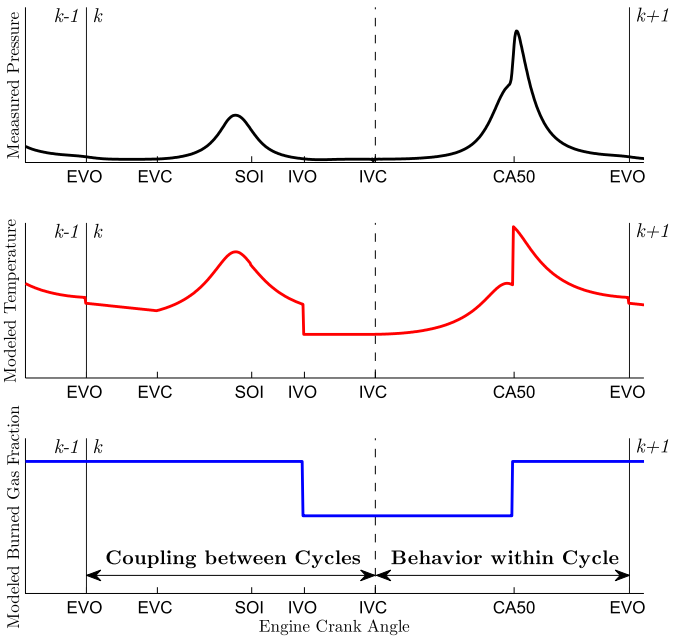

Fig. 4. Evolution of the measured in-cylinder pressure, modeled charge temperature, and modeled burned gas fraction. The thermal and composition coupling between cycles is modeled in the recompression region.

The discrete-time model developed in this section has two dynamic states to capture the interactions between cycles.

1) Temperature of the blowdown gases (T_{bd}), representing thermal dynamics.
2) Burned gas fraction of the blowdown gases (b_{bd}), representing composition dynamics. The burned gas fraction is the mass fraction of cylinder charge that is neither fuel nor air. For a more detailed discussion, please refer to Appendix.

The blowdown process refers to the rapid equalization of the cylinder pressure and the exhaust runner pressure just after exhaust valve opening (θ_{evo}). As seen in the typical recompression HCCI pressure trace in Fig. 2, the states are defined after blowdown, at θ_{evo}.

The dynamic evolution of the states can be broken down into two phases—the coupling between the cycles, and the behavior within the cycle. An overview of this dynamic evolution is presented in Fig. 4. The model equations for these two phases are presented in Sections IV-A and IV-B.

A. Coupling Between Cycles

In recompression HCCI, a large fraction of the in-cylinder charge is trapped before it can be exhausted. The hot residual gases retained between engine cycles have a significant impact on the temperature and composition of the in-cylinder charge of the subsequent cycle. This internal coupling between cycles is quantified by the residual gas fraction (x_r), which is defined as the mass fraction of the charge that is trapped during NVO

$$x_r(k) = \frac{\text{Mass of residuals}}{\text{Mass of charge}} = \frac{m_{\text{res}}(k)}{m_c(k)}. \tag{2}$$

The residual gas fraction cannot be measured directly, but is estimated by pressure trace analysis to be very large in the current application, between 50% and 70%. Correctly predicting the amount, temperature and composition of these residual gases is the key to modeling the recompression HCCI process. For a given exhaust valve closing timing u_{evc}, temperature of blowdown gases T_{bd}, engine speed ω, and pressure ratio across the engine Π, the residual gas fraction is regressed as

$$x_r(k) = 1 - (\alpha_0 + \alpha_1 u_{\text{evc}})\, \Pi^{\alpha_2} T_{\text{bd}}(k)^{\alpha_3} \omega(k)^{\alpha_4} \tag{3}$$

where

$$\Pi = \frac{p_{\text{im}}(k)}{p_{\text{em}}(k)}.$$

Parameters $\alpha_{0,\ldots,4}$ are tuned to fit heat release analysis results.

1) Composition Coupling: The burned gas fraction in the cylinder is assumed be at one of two levels—a value before (b_c) and after (b_{bd}) combustion. These are related by assuming that an x_r portion of the burned gases is trapped between cycles

$$b_c(k) = x_r(k) b_{\text{bd}}(k). \tag{4}$$

2) Thermal Coupling: Sensitivity analysis suggests that temperature is the dominant factor in determining the start of combustion in HCCI combustion [23]. Thus, modeling the evolution of charge temperature both between and within cycles is crucial in predicting combustion phasing θ_{50}.

After blowdown, a portion of the charge exits the cylinder through the exhaust valve. The cooling of the rest of the charge between θ_{evo} and u_{evc} is modeled by a scaling constant c_e. The trapped gases are polytropically compressed and expanded during the NVO region to obtain the residual gas temperature. Charge cooling due to the evaporation of the injected fuel (m_f^{inj}) is modeled at the start of injection angle (u_{soi})

$$T_{\text{evc}}(k) = c_e T_{\text{bd}}(k) \tag{5}$$

$$T_{\text{soi}}(k) = T_{\text{evc}}(k) \left(\frac{V_{\text{evc}}}{V_{\text{soi}}}\right)^{n-1} - \beta_0 m_f^{\text{inj}}(k) \tag{6}$$

$$T_{\text{res}}(k) = T_{\text{soi}}(k) \left(\frac{V_{\text{soi}}}{V_{\text{ivo}}}\right)^{n-1}. \tag{7}$$

The thermal coupling between cycles is modeled by an energy balance equation at θ_{ivc}. The temperature of the hot residuals is assumed to be T_{res} while the rest of the charge is considered to be at the intake manifold temperature (T_{im}). Assuming constant specific heats, energy balance leads to

$$T_{\text{ivc}}(k) = x_r(k) T_{\text{res}}(k) + (1 - x_r(k))\, T_{\text{im}}. \tag{8}$$

B. Behavior Within the Cycle

1) In-Cylinder Temperature: HCCI combustion is usually phased just after TDC, and heat release occurs fairly rapidly over a few crank angle degrees. Hence, the heat release can be approximated as a constant volume process. The instantaneous heat release at θ_{50} occurs between a polytropic compression from θ_{ivc} and a polytropic expansion to θ_{evo}. The charge

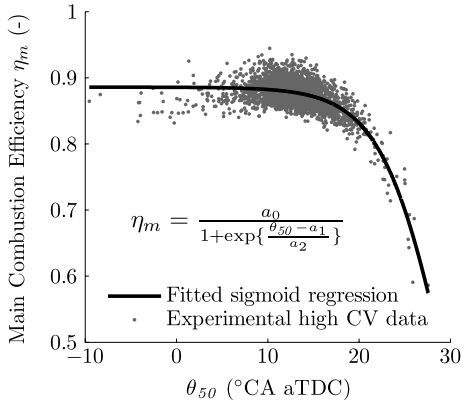

Fig. 5. Combustion efficiency η_m is modeled as a function of θ_{50}, similar to [34]. Combustion efficiency drops off sharply at late phasing conditions. The values of η_m are obtained through heat release analysis.

temperature after combustion ($T_{\rm ac}$) and the temperature rise due to combustion (ΔT) are given by

$$T_{\rm ac} = T_{\rm ivc}\left(\frac{V_{\rm ivc}}{V_{50}}\right)^{n-1} + \Delta T \tag{9}$$

$$\Delta T = \frac{\eta_m(k)\, q_{\rm lhv} m_f(k)}{c_v(k) m_c(k)} = \frac{\eta_m(k)\, q_{\rm lhv} R}{c_v(k)\, p_{\rm ivc} V_{\rm ivc}} m_f(k) T_{\rm ivc}(k) \tag{10}$$

where η_m is the combustion efficiency and n is the polytropic exponent. As seen in Fig. 5, η_m is roughly constant for most values of θ_{50}, and drops off sharply at late phasing conditions. The specific heat of combustion c_v varies as a function of composition (b_c) to capture variations in mixture properties

$$\eta_m(k) = \frac{\beta_1}{1+\exp\left\{\frac{\theta_{50}(k)-\beta_2}{\beta_3}\right\}}\left(1+\beta_4\omega(k)\right) \tag{11}$$

$$c_v(k) = 1+\beta_5 b_c(k). \tag{12}$$

The constants β_1, β_2, and β_3 are obtained from experimental data, see Fig. 5. Parameters β_4 and β_5 are tuned to fit data. The effect of engine speed on heat transfer losses is lumped into combustion efficiency, similar to [33].

Polytropic expansion after combustion and the ideal gas law give the charge conditions at $\theta_{\rm evo}$ to be

$$T_{\rm evo}(k) = T_{\rm ac}\left(\frac{V_{50}}{V_{\rm evo}}\right)^{n-1} = T_{\rm ivc}(k)\left(\frac{V_{\rm ivc}}{V_{\rm evo}}\right)^{n-1} \times\left[1+\frac{\eta_m\, q_{\rm lhv} R {V_{50}}^{n-1}}{c_v\, p_{\rm ivc} {V_{\rm ivc}}^{n}} m_f(k)\right] \tag{13}$$

$$p_{\rm evo}(k) = p_{\rm ivc}(k)\frac{V_{\rm ivc}}{V_{\rm evo}}\frac{T_{\rm evo}(k)}{T_{\rm ivc}(k)}. \tag{14}$$

Expansion is followed by the blowdown process, which is modeled as a polytropic expansion from the pressure at $\theta_{\rm evo}$ ($p_{\rm evo}$) to the exhaust manifold pressure ($p_{\rm em}$), with the polytropic exponent n. The temperature at blowdown ($T_{\rm bd}$) is

$$T_{\rm bd}(k+1) = T_{\rm evo}(k)\left(\frac{p_{\rm evo}}{p_{\rm em}}\right)^{\frac{1-n}{n}} = T_{\rm ivc}(k)\left(\frac{p_{\rm ivc}(k)}{p_{\rm em}}\right)^{\frac{1-n}{n}} \times\left[1+\frac{\eta_m\, q_{\rm lhv} R {V_{50}}^{n-1}}{c_v\, p_{\rm ivc} {V_{\rm ivc}}^{n}} m_f(k)\right]^{\frac{1}{n}}. \tag{15}$$

2) In-Cylinder Composition: The burned gas fraction before (b_c) and after ($b_{\rm bd}$) combustion can be related by algebraic relations that assume that the fuel combines with a stoichiometric mass of air to form an equivalent mass of burned gases

$$b_{\rm bd}(k+1) = \frac{(\,{\rm AFR}_s+1)\, m_f(k)}{m_c(k)} + b_c(k) = \frac{(\,{\rm AFR}_s+1)\, R}{p_{\rm ivc} V_{\rm ivc}} T_{\rm ivc}(k) m_f(k) + b_c(k). \tag{16}$$

C. Model Outputs

1) Combustion Phasing: Autoignition is predicted using the integrated Arrhenius rate threshold model. The combustion of the hydrocarbon fuel is approximated as a single-step global reaction with an Arrhenius-type reaction rate [35], using a fixed activation temperature ($B = E_a/R_u$) and preexponential factor (A). The integration is carried out until the Arrhenius threshold ($K_{\rm th}$) is hit at the start of combustion ($\theta_{\rm soc}$). Injecting earlier in the recompression region advances phasing approximately linearly, and is thus modeled to linearly reduce the integration threshold. The model can be expressed as follows:

$$K_{\rm th}(u_{\rm soi}) = k_0 - u_{\rm soi} = \int_{\theta_{\rm ivc}}^{\theta_{\rm soc}} \frac{A}{\omega} p_c(\theta)^{n_p} \exp\left(\frac{B}{T_c(\theta)}\right) {\rm d}\theta \tag{17}$$

where ω is the engine speed and k_0, n_p are model parameters. The pressure (p_c) and temperature (T_c) of the charge in the cylinder are given by a polytropic compression with a polytropic exponent n

$$p_c(\theta) = p_{\rm ivc}\left(\frac{V_{\rm ivc}}{V(\theta)}\right)^{n}, \quad T_c(\theta) = T_{\rm ivc}\left(\frac{V_{\rm ivc}}{V(\theta)}\right)^{n-1}. \tag{18}$$

In this paper, $\theta_{\rm soc}$ is considered to be θ_{02}, the engine crank angle at which 2% of the total heat release occurs. The output θ_{50} is modeled as a linear function of $\theta_{\rm soc}$

$$\theta_{50} = \gamma_1\theta_{\rm soc} + \gamma_0 \tag{19}$$

where γ_0 and γ_1 are constants obtained from heat release analysis. The model is similar in form to the integral threshold method used to predict SI engine knock, see for example [36].

2) Cycle-Averaged Mass Flows: In lean HCCI combustion, there is a difference between the air–fuel equivalence ratio λ that is measured in the exhaust (λ_m) and the lambda actually in the cylinder (λ_c), even at steady-state conditions. The trapped residual gases contain oxygen that does not leave the cylinder, and is subsequently not measured by the lambda sensors in the exhaust, with $\lambda_m < \lambda_c$.

The mass of air that is inducted in the cylinder ($m_{\rm air}^{\rm meas}$), and that is actually in the cylinder ($m_{\rm air}$) are determined by considering the appropriate fractions of the total mass of charge. The mass of charge (m_c) is determined by the ideal gas law

$$m_{\rm air} = (1-b_c)\, m_c - m_f \tag{20}$$

$$m_{\rm air}^{\rm meas} = (1-x_r)\, m_c - m_f \tag{21}$$

$$m_c = \frac{p_{\rm ivc} V_{\rm ivc}}{R T_{\rm ivc}}. \tag{22}$$

TABLE II
LINEARIZATION OPERATION POINT

Quantity	Nominal point	Quantity	Nominal point
u_{evc}	253 °CA aTDC	T_{bd}	657 K
m_f^{inj}	11.2 mg/cycle	b_{bd}	0.88
u_{soi}	330 °CA bTDC	p_{im}	1.1 bar
θ_{50}	7.99 °CA aTDC	p_{em}	1.01 bar
ω	1800 rpm		

Finally the air–fuel equivalence ratios are given by

$$\lambda_c = \frac{1}{\mathrm{AFR}_s} \cdot \frac{m_{\mathrm{air}}}{m_f} = \frac{1}{\mathrm{AFR}_s} \cdot \left[(1 - b_c) \frac{m_c}{m_f} - 1 \right] \quad (23)$$

$$\lambda_m = \frac{1}{\mathrm{AFR}_s} \cdot \frac{m_{\mathrm{air}}^{\mathrm{meas}}}{m_f} = \frac{1}{\mathrm{AFR}_s} \cdot \left[(1 - x_r) \frac{m_c}{m_f} - 1 \right]. \quad (24)$$

From (23) and (24), the model predicts $\lambda_m < \lambda_c$, since $x_r > b_c$ for lean combustion.

D. Linearized Model

The nonlinear system of equations given by (2)–(24) is linearized about the nominal operating point specified in Table II. The linearization point was chosen to be a typical HCCI operating point at a nominal engine speed (1800 r/min). The specific values of the inputs (m_f^{inj}, u_{soi}, u_{evc}) and the outputs (θ_{50} and IMEP) were chosen to be approximately in the middle of their observed usable ranges. The actuator settings were reasonably far away from the saturation constraints, and θ_{50} was chosen to be away from both the ringing and the high variability regions. This linearized model is used to develop the model-based feedforward controller and the state observer

$$\begin{aligned} x(k+1) &= Ax(k) + \begin{bmatrix} B_{\mathrm{soi}} & B_{\mathrm{evc}} & B_f & B_\omega \end{bmatrix} u(k) \\ \theta_{50}(k) &= Cx(k) + \begin{bmatrix} D_{\mathrm{soi}} & D_{\mathrm{evc}} & D_f & D_\omega \end{bmatrix} u(k) \\ u(k) &= \begin{bmatrix} u_{\mathrm{soi}}(k) & u_{\mathrm{evc}}(k) & m_f^{\mathrm{inj}}(k) & \omega(k) \end{bmatrix}^T \\ x(k) &= [T_{\mathrm{bd}}(k) \quad b_{\mathrm{bd}}(k)]^T \end{aligned} \quad (25)$$

where

$$\begin{aligned} A &= \begin{bmatrix} 0.496 & -90.63 \\ -1.27 \times 10^{-4} & 0.546 \end{bmatrix} \\ B &= \begin{bmatrix} 0.012 & -1.49 & 17.55 & 0.041 \\ 0 & -.004 & 0.0355 & 0 \end{bmatrix} \\ C &= [-0.1213, 0], \; D = [-0.0914, 0.56, 0.19, -0.0023]. \end{aligned} \quad (26)$$

For the chosen linearization point, both discrete eigenvalues of the model are stable and lie on the positive real axis within the unit circle. The location of these eigenvalues moves for different choices of the linearization point.

Experiments show that reducing x_r (for example, by phasing u_{evc} later) results in later combustion phasing θ_{50}, and in the onset of oscillatory dynamics leading to significant CV [21], [37]. The model presented here captures these results qualitatively. At late phasing conditions one of the eigenvalues crosses over to the left half plane, which predicts oscillatory dynamics. Future work is focused on correctly predicting both the onset and nature of this variability through an additional chemical coupling state introduced by the combustion of unburned fuel in the NVO region.

V. MODEL VALIDATION

Model coefficients were determined using a least squares optimization process. Data to parameterize the control-oriented model was taken from the experimental setup described in Section II. Heat release analysis results were compared to the control-oriented model predictions.

A. Steady-State Parameterization

The control-oriented model was parameterized using steady-state data recorded at intake manifold pressure of 1.1 bar. Fig. 6 presents steady-state parameterization results of three performance outputs (θ_{50}, IMEP, and m_{air}) for four actuator sweeps (u_{evc}, u_{soi}, m_f^{inj}, and ω). The most important output, combustion phasing θ_{50}, is plotted in the top row. The θ_{50} trends are predicted well for all four actuator sweeps, except for very early u_{evc}. However, the engine is typically not run in this actuator range, except at very low load conditions. For the overall data set, θ_{50} is predicted with an RMS error of 0.81 °CA. This is considered to be adequately good performance.

Injecting early in the recompression region increases pumping work and reduces IMEP. In the interest of reducing model parameters, this effect is not captured in the current model. This does not affect the performance of the model for developing combustion phasing controllers.

B. Transient Validation

The accuracy of the fuel governor control strategy depends on the control-oriented model correctly predicting the dynamic behavior of the engine. The setup outlined in Fig. 7 was used to test the model's closed-loop transient behavior. A mid-ranging feedback controller, see Section VI-A, was implemented both in simulation and on the rapid prototyping hardware. Identical desired load and $\theta_{50}^{\mathrm{ref}}$ input steps were fed to both the model and the engine. Since constraints on future-predicted actuator trajectories are used in the fuel governor control strategy, it is important to verify the transient validity of both the simulated actuator and output trajectories. The predicted θ_{50}, u_{evc}, and u_{soi} traces were compared with engine measurements.

The results of this test, shown in Fig. 8, demonstrate satisfactory closed loop model validation of the model. These plots compare experimental transient results with model predictions. The predicted θ_{50} and u_{soi} traces match both the magnitude and dynamic behavior of the engine measurements. These closed loop validation results support the use of this model for predictive model-based control.

The offset seen in the u_{evc} predictions in Fig. 8 is attributed to several months of engine ageing, and to unmodeled environmental factors. For example, the coolant temperatures for the parameterization data set and the experiments are different. Also, the feedback structure of the controller assigns any error in model prediction to u_{evc}. In spite of this offset, the dynamic behavior of the engine u_{evc} is reproduced correctly.

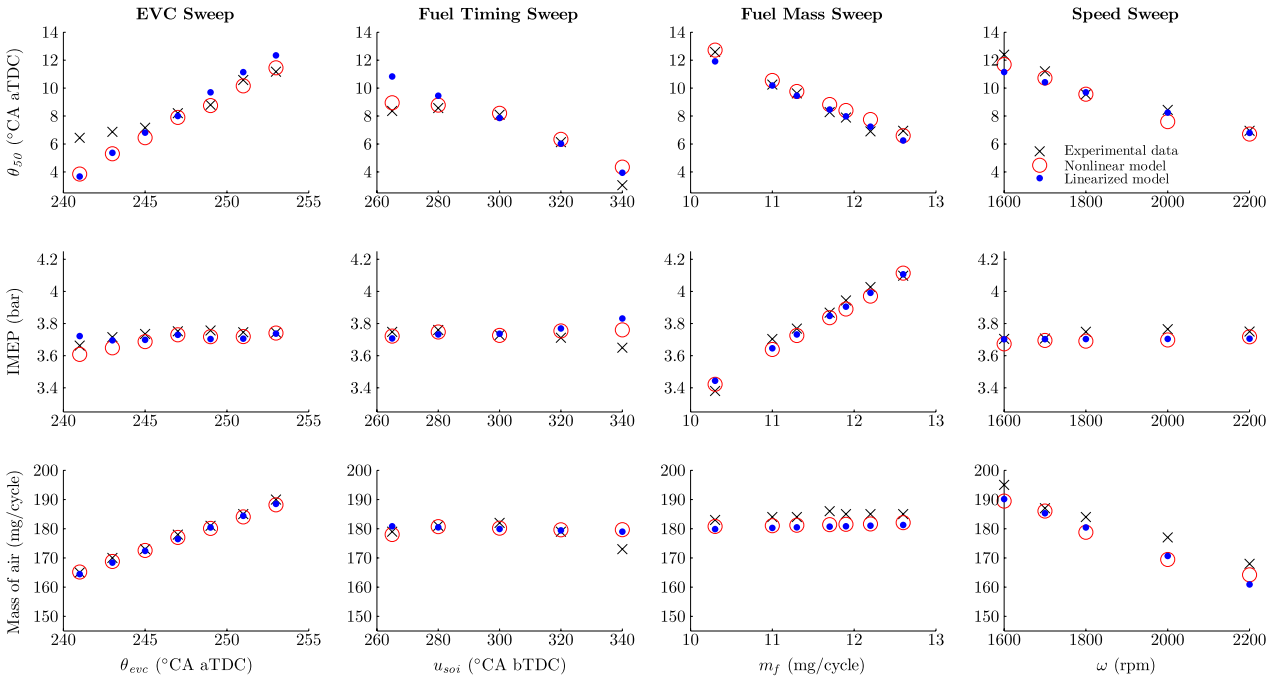

Fig. 6. Steady-state parameterization results of three performance outputs (θ_{50}, IMEP, and m_{air}) for four actuator sweeps (u_{evc}, u_{soi}, m_f^{inj}, and ω).

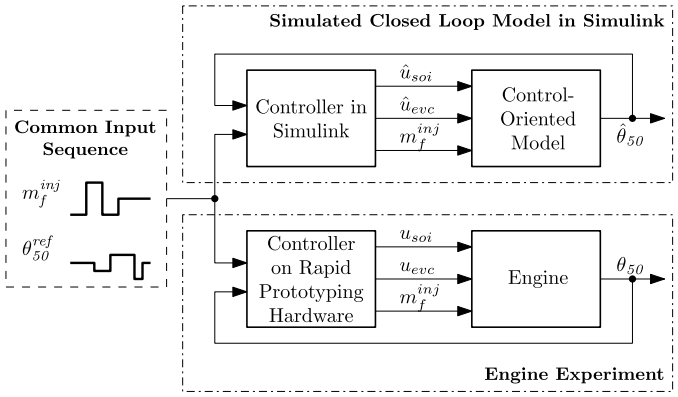

Fig. 7. Transient validation setup—identical desired load and θ_{50}^{ref} steps are fed to the closed-loop model and the engine. The predicted and measured θ_{50}, u_{soi}, and u_{evc} traces are compared.

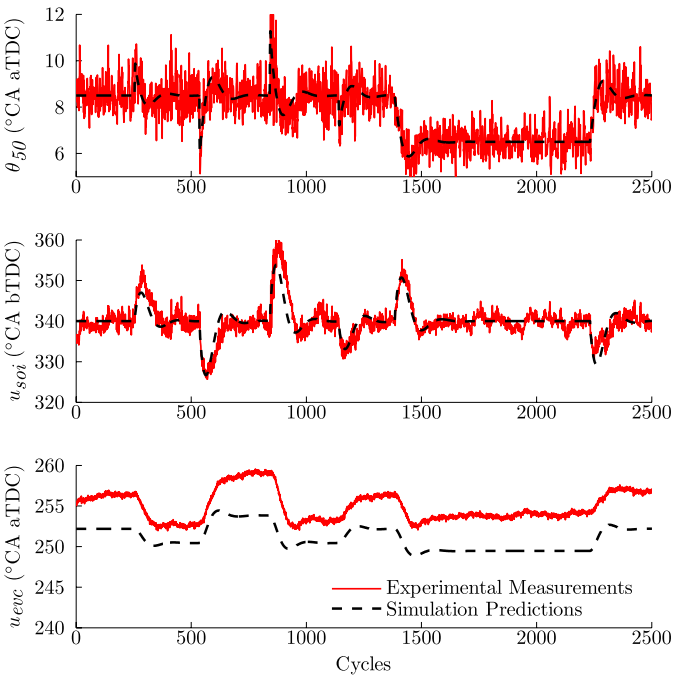

Fig. 8. Transient validation of model—identical desired load and θ_{50}^{ref} steps are fed to the model and the engine, as in Fig. 7. The model correctly predicts the magnitude and dynamic behavior of the engine measurements.

VI. Controller Design

The load range in recompression HCCI engines is bounded from below by high CV, and from above by ringing and constraints on pressure rise rates [4]. This paper aims to augment previous strategies that control u_{soi} and u_{evc} by shaping the m_f^{inj} command during large load transitions.

The two main performance outputs to be controlled are the engine load (IMEP) and the combustion phasing (θ_{50}). Engine load is a strong function of the mass of fuel injected (m_f^{inj}). Therefore a load transition m_f^{inj} is traditionally assumed to be externally specified, and is considered to be a disturbance for the combustion phasing controller. The combustion phasing controller regulates θ_{50} to a reference combustion phasing set-point (θ_{50}^{ref}), typically chosen to maximize fuel efficiency. This set-point is either determined offline, or is provided by a supervisory controller. Hence the combustion phasing controller design problem reduces to using u_{soi} (four values, one for each cylinder) and u_{evc} (a single value for the engine) to regulate θ_{50} during a m_f^{inj} transition.

An overview of the control strategy is presented in Fig. 1. The baseline controller from Section VI-A is a two-input single-output (TISO) feedback-feedforward controller that

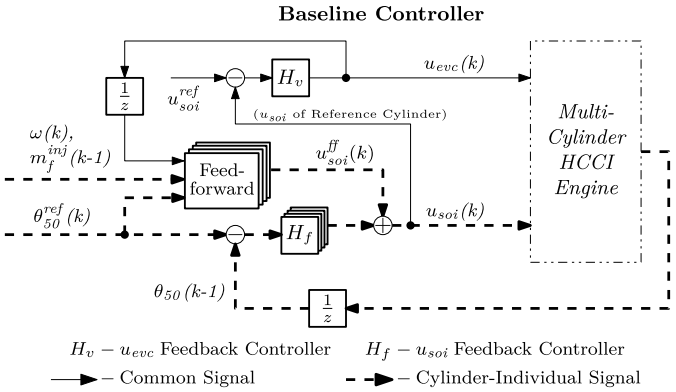

Fig. 9. Baseline controller—two inputs u_{soi} and u_{evc} in a midranging feedback configuration, with a model-based feedforward for u_{soi}.

uses u_{soi} and u_{evc} to regulate θ_{50}. The baseline controller works well during small load transitions, but exhibits unsatisfactory transient performance during larger transitions, even if the steady-state operating points of the transition lie within the acceptable phasing range. To solve this problem, a fuel governor is designed in Section VII to augment the baseline controller. The governor modifies the transient m_f^{inj} command during large load transitions, if future actuator constraint violations are predicted. Two variants of the fuel governor with differing computational complexity are presented.

A. Baseline Controller Design

The baseline TISO controller from Fig. 1 is presented in more detail in Fig. 9. It uses the u_{evc} and u_{soi} actuators to regulate θ_{50}, and comprises of a feedback loop and a model-based feedforward component of u_{soi}.

1) Feedback Loop: The feedback loop consists of two PI controllers arranged in a mid-ranging control configuration. Mid-ranging is a process control technique in which a coarse actuator and a fine actuator are coordinated to control a single feedback output [38]. This TISO control technique has been used in HCCI engine control applications, see [39], [40].

In the current application, the u_{evc} and u_{soi} actuators act as the coarse and fine actuators, respectively. The u_{evc} actuator has the larger range and greater authority. However, the hydraulic cam phasing actuator is relatively slow, and has a common value for all cylinders. In contrast, u_{soi} has limited range, but can be set independently from cycle-to-cycle for each cylinder. The θ_{50} tracking error signal drives a PI controller (H_f in Fig. 9) that controls u_{soi}. The slower u_{evc} moves or mid-ranges u_{soi} back toward its reference set point. This is accomplished using an integral controller (H_v in Fig. 9) driven by the u_{soi} tracking error for a fixed reference cylinder, here cylinder 1. Note that, in a multicylinder engine with a single cam phaser, this control strategy will regulate u_{soi} of only one cylinder to its reference set point.

As discussed in [8], a nonlinear least-squares optimization was carried out on the closed loop system with actuator dynamics to determine the optimal feedback controller gains. A typical set of θ_{50}^{ref} and m_f^{inj} input steps was used in the optimization process. The ability of the controller to track θ_{50}^{ref} was evaluated using a cost function that balanced tracking error and controller effort. Gains were detuned on the engine to ensure that they were not overly aggressive.

2) Model-Based Feedforward: Model-based feedforward is used for u_{soi} to speed up transient responses. The linearized model from Section IV-D is used to determine the steady-state fuel injection timing input ($u_{\text{soi}}^{\text{ss}}$) needed to attain the desired combustion phasing output θ_{50}^{ref}, assuming that the current values of all other inputs (here u_{evc} and m_f^{inj}) persist at steady state. The linearized model at steady state is inverted as follows:

$$\begin{aligned} x_{\text{ss}} &= Ax_{\text{ss}} + B_{\text{soi}}u_{\text{soi}}^{\text{ss}} + B_{\text{evc}}u_{\text{evc}} + B_f m_f^{\text{inj}} + B_\omega \omega \\ \theta_{50}^{\text{ref}} &= Cx_{\text{ss}} + D_{\text{soi}}u_{\text{soi}}^{\text{ss}} + D_{\text{evc}}u_{\text{evc}} + D_f m_f^{\text{inj}} + D_\omega \omega \therefore u_{\text{soi}}^{\text{ss}} \\ &= [0 \quad 1]\begin{bmatrix} (A-I) & B_{\text{soi}} \\ C & D_{\text{soi}} \end{bmatrix}^{-1} \\ &\quad \cdot \begin{bmatrix} -B_{\text{evc}} & -B_f & -B_\omega & 0 \\ -D_{\text{evc}} & -D_f & -D_\omega & 1 \end{bmatrix} \left[u_{\text{evc}}, m_f^{\text{inj}}, \omega, \theta_{50}^{\text{ref}}\right]^T. \end{aligned} \tag{27}$$

Here x_{ss} is the steady-state value of the states. The feedforward component (u_{soi}^{ff}) is set to be $u_{\text{soi}}^{\text{ss}}$. Hence, the feedforward block in Fig. 9 is a fixed gain. Since each cylinder can have distinct m_f^{inj} and θ_{50}^{ref} commands, and u_{evc} and ω vary continuously within the cycle, the controller generates four distinct values of the feedforward component of u_{soi} every cycle.

Note that the u_{evc} input in the feedforward equation given by (27) introduces a coupling between the slow and the fast actuators that may not exist in other midranging controllers seen in literature. This coupling is necessary in the current application for correct model-based inversion. Further, it can be shown through basic linear analysis that this feedforward term maintains the stability of the closed-loop system.

3) Experimental Validation of Baseline Controller: The baseline controller works well for small to mid load transitions, as seen in Fig. 10 where m_f^{inj} is stepped from 10.5 to 8.8 mg/cycle at cycle number 30. The torques for all four cylinders step smoothly from the initial to the final values without any spikes or dips. Note that the cylinder torques differ due to cylinder-to-cylinder variations in a multicylinder engine. The combustion phasing output θ_{50} is regulated to the set-point of 8.5 °CA aTDC, and stays within reasonable bounds during the load transition.

The controller outputs u_{soi} and u_{evc} in Fig. 10 demonstrate the typical response of the coarse and fine actuators in a mid-ranging control strategy. The initial transient response to the load transition lasts for a few engine cycles, and is almost entirely compensated for by the fast actuator u_{soi}. The sudden initial change in u_{soi} is due to the model-based feedforward. The slower actuator u_{evc} slowly returns u_{soi} to its reference set-point, which is roughly in the middle of its range of authority. The reference set-point here is 340 °CA aTDC. This mid-ranging of u_{soi} happens over tens of cycles.

As discussed earlier, only u_{soi} of cylinder 1 mid-ranges correctly to the reference set-point of 340 °CA aTDC. The single u_{evc} actuator for the entire engine is driven by the u_{soi} tracking error for a fixed reference cylinder, here cylinder 1.

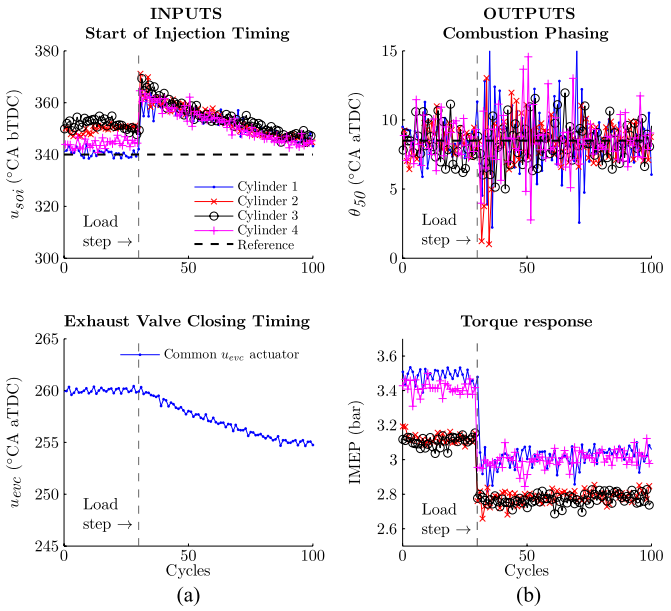

Fig. 10. Baseline controller—satisfactory transient response for small load steps (m_f^{inj}: 10.5 → 8.8 mg/cycle). (a) Controller inputs (u_{soi} and u_{evc}). (b) Performance outputs (θ_{50} and IMEP).

Equal amounts of fuel are commanded in each cylinder. Cylinder-to-cylinder variations result in different load levels for each cylinder. Although these imbalances can be compensated for by a feedback loop from m_f^{inj} to IMEP, this was not implemented in this paper to avoid disturbances from this loop.

VII. Fuel Governor

Large load transitions lead to large changes in the charge temperature, and consequently large undesired variations in combustion phasing. The baseline controller is unable to reject these variations in θ_{50}, as seen in Fig. 11. Here the baseline controller exhibits poor θ_{50} and IMEP tracking performance after a large load step down (m_f^{inj}: 11.4 → 8.8 mg/cycle). The fuel governor is added on to the controller-augmented system to improve this poor performance.

The fuel governor is a type of reference governor that modifies the desired fuel mass command ($m_f^{\text{des}}(k)$) by enforcing pointwise-in-time actuator constraints. The receding horizon principle is used to check for constraint violations, as summarized in Algorithm 1. Similar to [15], a bisectional search is carried out on the desired change in m_f^{inj} until the optimal change is found. This involves the optimization of a single parameter (β)

$$m_f^{\text{inj}}(k) = m_f^{\text{inj}}(k-1) + \beta \cdot (m_f^{\text{des}}(k) - m_f^{\text{inj}}(k-1)). \quad (28)$$

Ideally β is set to 1, in which case the fuel governor has no effect, and the desired fuel step is applied unmodified.

At every time step, the system is initialized at the current system states ($\hat{x}$), which are determined from a Luenberger observer designed using a linearized plant model. A model of the closed loop system is used to calculate future trajectories over a fixed future time horizon (N) with the fuel level maintained at $m_f^{\text{inj}}(k)$ calculated in (28). The parameter β is reduced if constraint violations are detected, and is increased

Algorithm 1 Bisectional Search to Maximize β in (28)

Input: Time horizon $N \geq 1$, tolerance $\epsilon \in [0, 1]$
Output: β in (28)

$i \leftarrow 1$, $\beta_0 \leftarrow 1$, $\beta_1 \leftarrow 1$, $\overline{\beta} \leftarrow 1$, $\underline{\beta} \leftarrow 0$
loop
  $m_f^{inj} \leftarrow m_f^{inj}(k-1) + \beta_i \cdot (m_f^{des}(k) - m_f^{inj}(k-1))$
  Simulate system over time horizon $\{k, \ldots, k+N\}$, initialized with current state of system $\hat{x}(k)$
  if Constraints are satisfied **then**
    if $(|\beta_i - \beta_{i-1}| \leq \epsilon)$ **then**
      return $\beta \leftarrow \beta_i$
    else
      $\underline{\beta} \leftarrow \beta_i$
    end if
  else
    $\overline{\beta} \leftarrow \beta_i$
  end if
  $i = i + 1$, $\beta_i = \frac{\underline{\beta}+\overline{\beta}}{2}$
end loop

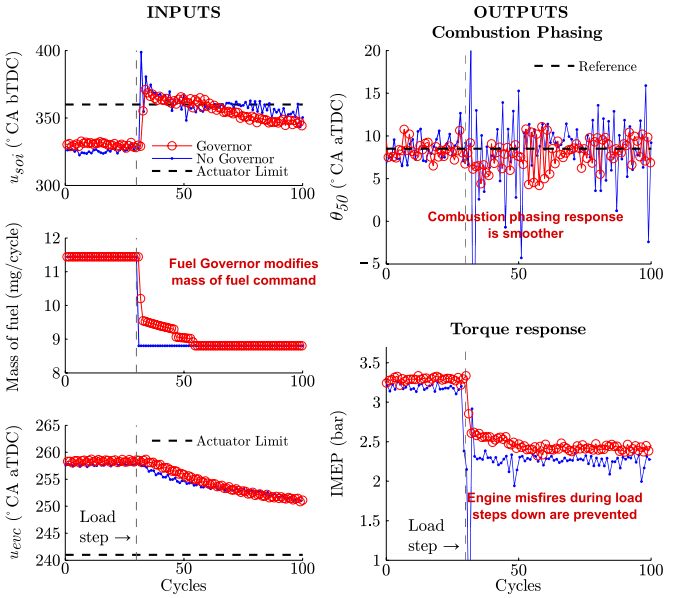

Fig. 11. Comparison between baseline controller and nonlinear fuel governor—improved θ_{50} and IMEP transient responses during load transitions, when the possibility of constraint violations exists. Results are presented for a single cylinder for clarity.

if all constraints are satisfied. The optimal value of $\beta \in [0, 1]$ is obtained subject to a predetermined convergence tolerance (ϵ). This process ensures that the tracking error between the desired and actual fuel levels is reduced. The governor performance depends on the fidelity of the plant model and the accuracy of the state observer.

The actuator constraints considered in this paper are saturation constraints (u_{soi}, u_{evc}) and rate constraints (u_{evc})

$$\begin{aligned} u_{\text{soi}}^{\min} &\leq u_{\text{soi}} \leq u_{\text{soi}}^{\max} \\ u_{\text{evc}}^{\min} &\leq u_{\text{evc}} \leq u_{\text{evc}}^{\max} \\ \Delta u_{\text{evc}}^{\min} &\leq \Delta u_{\text{evc}} \leq \Delta u_{\text{evc}}^{\max} \end{aligned} \quad (29)$$

where $\Delta u_{\mathrm{evc}}(k) = u_{\mathrm{evc}}(k) - u_{\mathrm{evc}}(k-1)$. The effect of u_{soi} is approximately linear in the NVO region, with the effect saturating for very late or very early injection. The u_{soi} saturation constraints are set to limit u_{soi} within this linear region. The u_{evc} rate and saturation constraints are obtained from the limits of the actuator hardware. The tuning of the feedback gains determines which constraints are active. In this paper, it was observed that u_{soi} saturation was the primary active constraint, and it was violated before the u_{evc} constraints.

The fuel governor augments existing control architectures, and doesn't completely replace them. This enables separation of control tasks, simplifying the overall control design. For example, in the current application, the combustion phasing regulation problem is handled by the baseline controller using u_{soi} and u_{evc}, while the actuator constraint enforcement task is handled by the fuel governor that modifies m_f^{inj}.

Further, the governor optimizes a single variable (β) to find the desired fuel trajectory. Optimizing a single variable is less complex, easier to implement, and computationally cheaper than other online optimization schemes such as model-predictive control of all actuators.

The overall effect of the governor is to act as a model-based filter with a variable time constant that slows down large m_f^{inj} steps. This effect can be mimicked by a heuristic solution such as a low-pass filter with a lookup table of gains. However, this requires calibration effort to ensure that the slowing down of m_f^{inj} is not too conservative (which would lead to overly slow transitions) or too aggressive (which could lead to misfire and excessive θ_{50} variation). In this case, the governor can be used in simulation to tune the filter gains.

A. Nonlinear Fuel Governor

The nonlinear fuel governor uses the nonlinear HCCI combustion model to predict future trajectories. This strategy was implemented on the rapid prototyping hardware and was used to regulate θ_{50} during load transitions. The main advantages of this strategy, as validated by experiments are as follows.

1) Improved θ_{50} and IMEP transient responses during load transitions, when constraint violations are predicted.
2) Larger load transitions than were possible with the baseline controller alone.

1) Improved Performance During Larger Load Transitions: Fig. 11 compares the performance for the baseline controller and the nonlinear fuel governor for a larger load transition than the one considered in Fig. 10. Here m_f^{inj} is stepped from 11.4 to 8.8 mg/cycle at cycle number 30. The baseline controller tries to compensate for the large charge temperature drop caused when m_f^{inj} drops suddenly in a single cycle. Significant variability in the θ_{50} and IMEP responses is seen immediately after the load transition. The combustion phasing response is rough and oscillatory. The torque output drops sharply, indicating incomplete combustion and misfire. The engine continued to run in the experimental dynamometer environment, but this could cause an unacceptable engine stall in a vehicle.

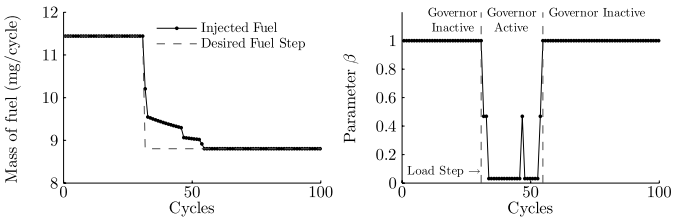

Fig. 12. Variation in fuel governor parameter β during a typical load transient.

In contrast, the nonlinear fuel governor demonstrates significantly improved θ_{50} and IMEP transients. The combustion phasing response is less oscillatory, and engine misfires are prevented. The result is a smoother torque transition during the load step down. The fuel governor achieves these improvements by slowing down the m_f^{inj} command when future actuator constraint violations are predicted. In this case, the actuator constraint that is active is u_{soi} saturation.

It is seen that u_{soi} slightly exceeds the actuator limit. Some of the design choices made to reduce complexity increase errors in the actuator position predictions. The control-oriented model does not fully represent engine behavior. Further, the nonlinearities inherent in the system cause increased errors in the state estimated by the linear observer away from the nominal operating point. The constraints have to be made more conservative to account for these.

Given the desired m_f^{des} and actual m_f^{inj} trajectories, the value of parameter β in the fuel governor is given by

$$\beta(k) = \frac{m_f^{\mathrm{inj}}(k) - m_f^{\mathrm{inj}}(k-1)}{m_f^{\mathrm{des}}(k) - m_f^{\mathrm{inj}}(k-1)}. \tag{30}$$

Fig. 12 shows a typical fuel governor m_f^{inj} transient and the associated β plot. A large portion of the step happens in the first cycle. The size of this step is limited by the active constraint (here u_{soi} saturation). The optimal value of $\beta \in [0, 1]$ is obtained subject to the convergence tolerance (ϵ).

In general, tip-in responses are not as challenging as tip-out responses. The increased fuel amount and temperatures lead to earlier combustion phasing. This can cause ringing without the governor, but not combustion failures or misfires. Hence the potential improvement shown by the governor is less dramatic.

2) Extending the Load Transition Range: The nonlinear fuel governor enables larger load transitions than were possible with the baseline controller. An example of this is shown in Fig. 13 for a m_f^{inj} transition from 12.3 to 8.8 mg/cycle at cycle number 30. Instead of m_f^{inj} stepping in a single cycle, the transition occurs over a few cycles, leading to smooth torque and combustion phasing responses. As discussed previously, the actuator constraints have to be made more conservative than their actual values. At these operating conditions, a commanded u_{soi} maximum limit of 360 °CA bTDC corresponds to an experimentally observed limit of 375 °CA bTDC.

VIII. Linearized Fuel Governor

The nonlinear fuel governor can be computationally expensive. The optimization of β in (28) must be run in real-

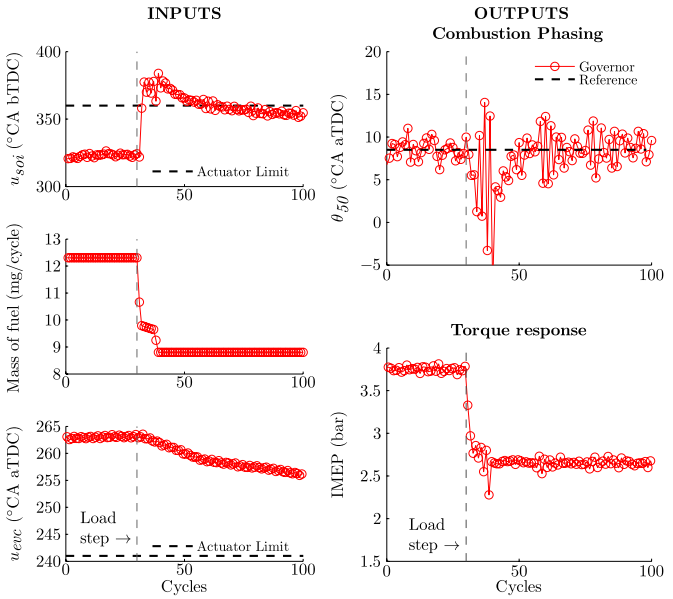

Fig. 13. Nonlinear fuel governor—larger load transitions than were possible with the baseline controller alone. Here m_f^{inj}: 12.3–8.8 mg/cycle.

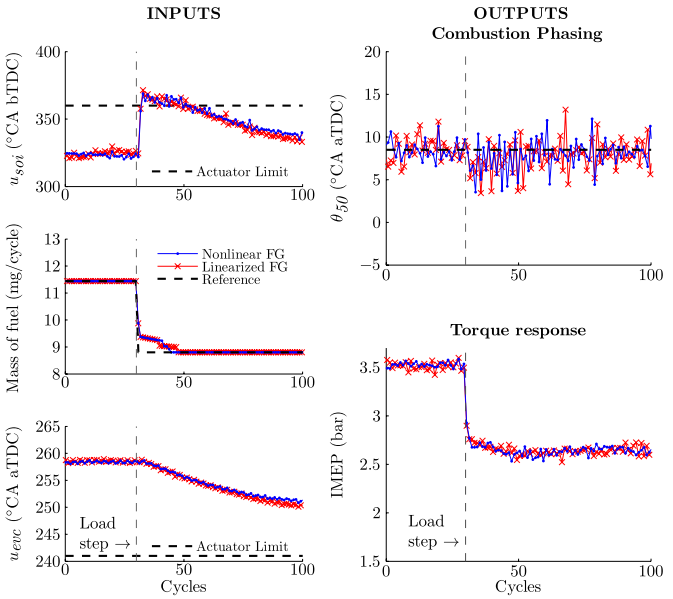

Fig. 14. Comparison between nonlinear and linearized fuel governor. The performance of both governors is very similar. Here m_f^{inj}: 11.4–8.8 mg/cycle.

time four times a cycle, to determine the m_f^{inj} input for every cylinder. Depending on the engine speed, the values of the time horizon (N), and the convergence tolerance (ϵ) in Algorithm 1, the nonlinear prediction model may have to be run several thousand times every second. In this application, the nonlinear fuel governor code was optimized to run in real-time on the experimental hardware. However, using the nonlinear prediction model in the governor may be infeasible on less computationally powerful engine control hardware.

To reduce computational load, the nonlinear prediction model is linearized about a chosen operating point. The procedure summarized in Algorithm 1 remains the same. In Fig. 14, the same m_f^{inj} transition from 11.4 to 8.8 mg/cycle is carried out for the nonlinear and the linearized fuel governors. The performance of both governors is very similar. The torque transition is smooth and there are no undue fluctuations in θ_{50} during the transition. Alternative schemes to speed up reference governor computation times are discussed in literature, see [16], [41].

A. Experimental Runtime Comparison

All fuel governor variants presented in this paper run in real-time. Profiling the nonlinear model suggested that the Arrhenius integral from (17) was the most computationally expensive part of the model. Replacing the Arrhenius integral with a lookup table led to an appreciable runtime improvement. Similarly the cylinder volume calculation was replaced by a lookup table. The linearized fuel governor showed a further drastic reduction in runtime.

Table III shows the typical maximum runtime for different control strategies for a standard series of load transitions. The typical additional computational overhead of augmenting the baseline controller with the linearized fuel governor is only 4%. Implementing the linearized fuel governor on less computationally powerful commercial engine control hardware should be feasible, and is planned in future work.

TABLE III
COMPARISON OF EXPERIMENTALLY RECORDED MAXIMUM RUNTIMES. A STANDARD TEST CYCLE WAS RUN FOR EACH CONTROL STRATEGY

Control Strategy	Maximum Runtime	Normalized Maximum Runtime
Nonlinear Fuel Governor (Arrhenius integral)	8.916 ms	7315%
Nonlinear Fuel Governor (lookup table)	2.315 ms	1900%
Linearized Fuel Governor	0.1271 ms	104%
Baseline Controller	0.1219 ms	100%

B. Load Steps at Different Engine Speeds

It is important to verify that the linearized fuel governor performs well for a range of speeds and loads. The same m_f^{inj} transition from 11.55 to 8.9 mg/cycle is carried out at 1600, 1800, and 2000 r/min, with results presented in Fig. 15. The nominal engine speed for the linearized model is 1800 r/min. The governor performs well for this variation in engine speed. The torque steps smoothly from the first operating point to the next, and there are no significant oscillations in the combustion phasing response.

C. Traversing from Stable to Oscillatory Dynamics After Load Transition Down

Fig. 16 shows the fuel governor response of different cylinders for the same load step down studied in Fig. 11. It illustrates that while the transient response of some cylinders can be excellent, other cylinders sometimes exhibit high cyclic

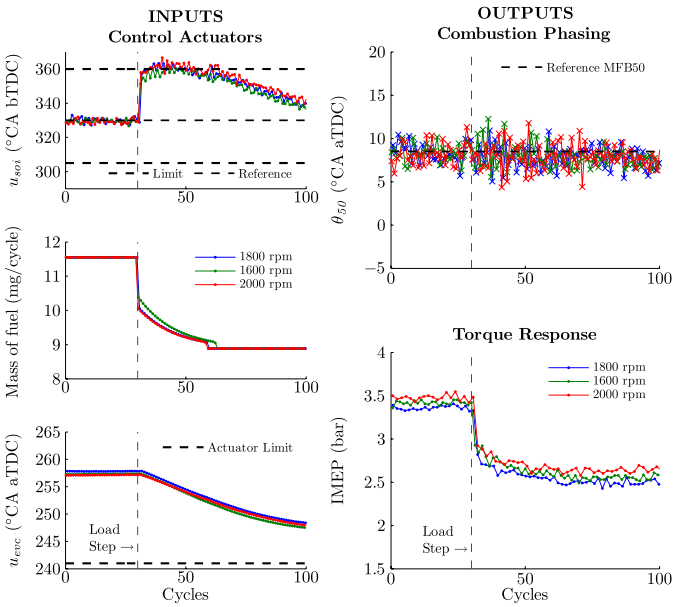

Fig. 15. Linearized fuel governor—results for different engine speeds.

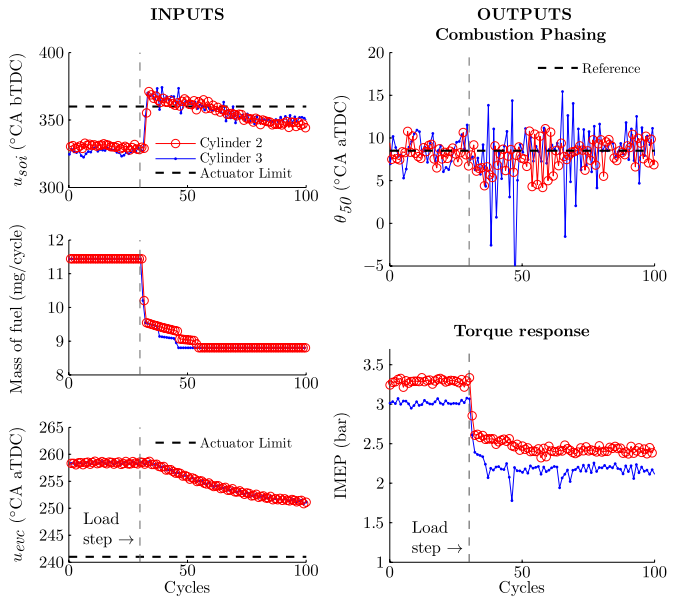

Fig. 16. Potential cylinder to cylinder variation in fuel governor response to load transition down.

variability in θ_{50}, specifically at lower loads. The initial IMEP and θ_{50} response just after the load transition is satisfactory for both cylinders, which indicates that the fuel governor improves transition performance for all cylinders. However, a few cycles after the load transition, the θ_{50} of cylinder 3 enters an oscillatory region, causing noticeable dips in IMEP. Note that most of the load transition is completed before the oscillations begin.

Cylinder-to-cylinder imbalances in load are not the primary cause of these oscillations. As shown in [3] and [21], late phasing HCCI combustion dynamics are oscillatory for both single and multicylinder engines. These oscillations are shown to be driven by the chemical energy coupling between cycles due to unburned fuel. The onset of the oscillatory dynamics varies with load and cylinder, as seen in Fig. 16. During the load transition, cylinder 3 (which has a lower load for the same m_f^{inj}) entered this oscillatory region while cylinder 2 did not. The model in this paper does not consider these unburned fuel dynamics.

As seen in [42] and later in [43], feedback gains designed for stable HCCI dynamics are destabilizing when applied in the oscillatory region, which suggests the need to improve the baseline controller. The authors have presented models [3], [21] and controllers [37] to capture and reduce these late-phasing oscillations in both single and multicylinder engines. The baseline controller will be extended in future work to incorporate this knowledge. The performance gains of the fuel governor can be further improved with a model that considers the unburned fuel dynamics and a baseline controller that globally stabilizes the engine phasing.

IX. Conclusion

Load transitions of varying magnitudes are experimentally controlled using model-based controllers. Load reductions are the focus of the experiments, as these can lead to unacceptable engine misfires.

The fuel governor is based on the reference governor concept that separates the closed loop design from the constraint enforcement requirement. The fuel governor-based strategies are experimentally shown to improve θ_{50} and IMEP transient responses during load transitions. The performance of the baseline controller is improved for load transitions where future constraint violations are predicted. Larger load transitions than were possible with the baseline controller alone are enabled. The linearized fuel governor is presented as a computationally efficient implementation of the governor. The typical additional computational overhead of augmenting the baseline controller with the linearized fuel governor is only 4%. Further, this control strategy is shown to work satisfactorily at different operating conditions.

The reference governor methodology can be extended to consider state-related constraints, such air-to-fuel ratio and pressure rise rate constraints. Future work includes implementation of the controllers on less computationally powerful commercial engine control hardware. Characterization of the onset of late phasing CV will be used to improve the performance of the baseline controller in dynamically oscillatory regions.

Appendix
Burned Gas Fraction

As seen in Fig. 17, the charge in the cylinder at any point of time is modeled as a mixture of three components–air, fuel, and burned gases. The chemical composition of these mixtures is determined from the stoichiometric combustion equation. For example, from (A.31), which represents the stoichiometric combustion of iso-octane, the constituents of the in-cylinder charge are considered to be.

1) Fuel (iso-octane): C_8H_{18}.
2) Air: $O_2 + 3.773N_2$.
3) Burned gases: $8CO_2 + 9H_2O + 47.16N_2$.

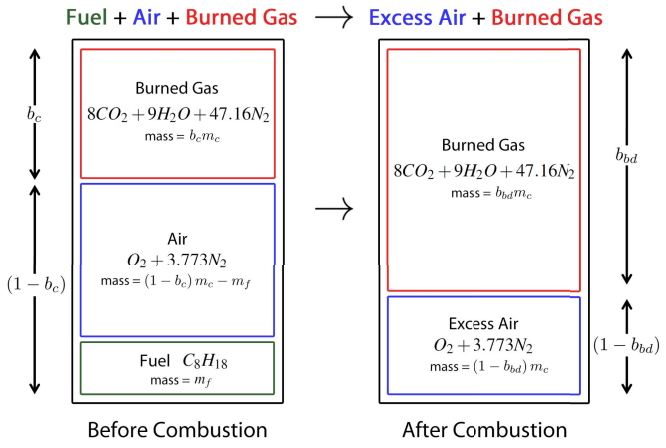

Fig. 17. Cylinder composition before and after combustion of iso-octane.

Note that the burned gas fraction is distinct from the residual gas fraction. Residual gases contain some leftover air after lean combustion. By definition, burned gases cannot contain any oxygen. In fact $b_c = b_{\text{bd}} x_r \implies b_c \leq x_r$.

The stoichiometric ($\lambda_c = 1$) and lean ($\lambda_c > 1$) combustion equations for iso-octane C_8H_{18} are given by

$$C_8H_{18} + 12.5\,(O_2 + 3.77N_2) \rightarrow 8CO_2 + 9H_2O + 47.16N_2 \tag{A.31}$$

$$\begin{aligned} C_8H_{18} + \frac{x_r}{1-x_r}(8CO_2 + 9H_2O + 47.16N_2) \\ + 12.5\lambda_c\,(O_2 + 3.77N_2) \rightarrow 12.5\,(\lambda_c - 1)\,(O_2 + 3.77N_2) \\ + \frac{1}{1-x_r}\,(8CO_2 + 9H_2O + 47.16N_2)\,. \end{aligned} \tag{A.32}$$

A. Molar Fraction of Oxygen

The molar fraction of oxygen (χ_{O2}) is an alternative measure of composition used in literature. It is defined as the ratio of the number of moles of oxygen to the total number of moles of reactants before combustion. This section develops the relationship between χ_{O2} and b_{bd}.

From (A.32) it is clear that if $\lambda_c > 1$, there is excess air in the exhaust. A portion of this excess air in the exhaust is recycled through the residual gases. As the composition of the residual gases and the gases after combustion is assumed to be the same, the ratio of the moles is also the ratio of the masses. The ratio of the masses is known to be x_r, by definition. This leads to the expression for χ_{O2} in terms of the in-cylinder air–fuel equivalence ratio λ_c and the residual gas fraction x_r. Finally, the air–fuel equivalence ratio λ_c can be expressed in terms of the burned gas fraction

$$\chi_{O2}(k) = \frac{N_{O2}}{N_{\text{total}}} = \frac{12.5\lambda_c(k)}{1 + 59.66\lambda_c(k) + \frac{64.16x_r(k)}{1-x_r(k)}} \tag{A.33}$$

$$\lambda_c(k) = \frac{1}{\text{AFR}_s} \cdot \left[(1 - b_c(k))\,\frac{m_c}{m_f} - 1\right] \tag{A.34}$$

$$m_c(k) = \frac{p_{\text{ivc}} V_{\text{ivc}}}{R T_{\text{ivc}}(k)}. \tag{A.35}$$

Equations (A.33)–(A.35) express the molar fraction of oxygen (χ_{O2}) in terms of the burned gas fraction state.

REFERENCES

[1] M. Yao, Z. Zheng, and H. Liu, "Progress and recent trends in homogeneous charge compression ignition (HCCI) engines," *Progr. Energy Combust. Sci.*, vol. 35, no. 5, pp. 398–437, Oct. 2009.

[2] F. Zhao, T. N. Asmus, D. N. Assanis, J. E. Dec, J. A. Eng, and P. M. Najt, *Homogeneous Charge Compression Ignition (HCCI) Engines—Key Research and Development Issues*. Warrendale, PA, USA: SAE International, 2003.

[3] E. Hellström, A. Stefanopoulou, J. Vavra, A. Babajimopoulos, D. Assanis, L. Jiang, *et al.*, "Understanding the dynamic evolution of cyclic variability at the operating limits of HCCI engines with negative valve overlap," *SAE Int. J. Eng.*, vol. 5, no. 3, pp. 995–1008, 2012.

[4] L. Manofsky, J. Vavra, D. Assanis, and A. Babajimopoulos, "Bridging the gap between HCCI and SI: Spark-assisted compression ignition," SAE Technical Paper 2011-01-1179, 2011, doi: 10.4271/2011-01-1179.

[5] J. Bengtsson, P. Strandh, R. Johansson, P. Tunestål, and B. Johansson, "Model predictive control of homogeneous charge compression ignition (HCCI) engine dynamics," in *Proc. IEEE Int. Conf. Control Appl.*, Oct. 2006, pp. 1675–1680.

[6] C.-J. Chiang and C.-L. Chen, "Constrained control of homogeneous charge compression ignition (HCCI) engines," in *Proc. 5th IEEE Conf. Ind. Electron. Appl.*, Jun. 2010, pp. 2181–2186.

[7] N. Ravi, H.-H. Liao, A. F. Jungkunz, A. Widd, and J. C. Gerdes, "Model predictive control of HCCI using variable valve actuation and fuel injection," *Control Eng. Pract.*, vol. 20, no. 4, pp. 421–430, 2012.

[8] S. Jade, E. Hellström, L. Jiang, and A. Stefanopoulou, "Fuel governor augmented control of recompression HCCI combustion during large load transients," in *Proc. Amer. Control Conf.*, Jun. 2012, pp. 2084–2089.

[9] S. Jade, E. Hellström, J. Larimore, L. Jiang, and A. Stefanopoulou, "Enabling large load transitions on multicylinder recompression HCCI engines using fuel governors," in *Proc. Amer. Control Conf.*, Jun. 2013, pp. 4423–4428.

[10] P. Kapasouris, M. Athans, and G. Stein, "Design of feedback control systems for stable plants with saturating actuators," in *Proc. 27th IEEE Conf. Decision Control*, Dec. 1988, pp. 469–479.

[11] E. G. Gilbert and K. T. Tan, "Linear systems with state and control constraints: The theory and application of maximal output admissible sets," *IEEE Trans. Autom. Control*, vol. 36, no. 9, pp. 1008–1020, Sep. 1991.

[12] E. Gilbert, I. Kolmanovsky, and K. Tan, "Discrete-time reference governors and the nonlinear control of systems with state and control constraints," *Int. J. Robust Nonlinear Control*, vol. 5, no. 5, pp. 487–504, 1995.

[13] A. Casavola and E. Mosca, "Reference governor for constrained uncertain linear systems subject to bounded input disturbances," in *Proc. 35th Conf. Decision Control*, Dec. 1996, pp. 3531–3536.

[14] A. Bemporad, "Reference governor for constrained nonlinear systems," *IEEE Trans. Autom. Control*, vol. 43, no. 3, pp. 415–419, Mar. 1998.

[15] J. Sun and I. Kolmanovsky, "Load governor for fuel cell oxygen starvation protection: A robust nonlinear reference governor approach," *IEEE Trans. Control Syst. Technol.*, vol. 13, no. 6, pp. 911–920, Nov. 2005.

[16] A. Vahidi, I. Kolmanovsky, and A. Stefanopoulou, "Constraint management in fuel cells: A fast reference governor approach," in *Proc. Amer. Control Conf.*, vol. 6. 2005, pp. 3865–3870.

[17] V. Tsourapas, J. Sun, and A. Stefanopoulou, "Incremental step reference governor for load conditioning of hybrid fuel cell and gas turbine power plants," in *Proc. Amer. Control Conf.*, Jun. 2008, pp. 2184–2189.

[18] J. M. Elder, J. T. Boys, and J. L. Woodward, "Integral cycle control of stand-alone generators," *IEE Proc. C, Generat. Transmiss. Distrib.*, vol. 132, no. 2, pp. 57–66, Mar. 1985.

[19] D. Henderson, "An advanced electronic load governor for control of micro hydroelectric generation," *IEEE Trans. Energy Convers.*, vol. 13, no. 3, pp. 300–304, Sep. 1998.

[20] I. Kolmanovsky, E. Gilbert, and J. Cook, "Reference governors for supplemental torque source control in turbocharged diesel engines," in *Proc. Amer. Control Conf.*, Jun. 1997, pp. 652–656.

[21] E. Hellström, J. Larimore, A. G. Stefanopoulou, J. Sterniak, and L. Jiang, "Quantifying cyclic variability in a multicylinder HCCI engine with high residuals," *J. Eng. Gas Turbines Power*, vol. 134, no. 11, pp. 112803-1–112803-8, 2012.

[22] R. Fitzgerald, R. Steeper, J. Snyder, R. Hanson, and R. Hessel, "Determination of cycle temperature and residual gas fraction for HCCI negative valve overlap operation," *SAE Int. J. Eng.*, no. 3, no. 1, pp. 124–141, 2010.

[23] C.-J. Chiang and A. G. Stefanopoulou, "Sensitivity analysis of combustion timing of homogeneous charge compression ignition gasoline engines," *J. Dyn. Syst. Meas. Control*, vol. 131, no. 1, pp. 014506-1–014506-5, 2009.
[24] J. Willand, R.-G. Nieberding, G. Vent, and C. Enderle, "The knocking syndrome—Its cure and its potential," SAE Technical Paper 982483, 1998, doi: 10.4271/982483.
[25] A. Babajimopoulos, P. V. Challa, G. A. Lavoie, and D. Assanis, "Model-based assessment of two variable cam timing strategies for HCCI engines: Recompression vs. rebreathing," in *Proc. ASME Int. Combust. Eng. Division Spring Tech. Conf.*, 2009, pp. 597–610.
[26] R. P. Fitzgerald and R. Steeper, "Thermal and chemical effects of NVO fuel injection on HCCI combustion," *SAE Int. J. Eng.*, vol. 3, pp. 46–64, Aug. 2010.
[27] N. Ravi, H.-H. Liao, A. F. Jungkunz, C.-F. Chang, H. H. Song, and J. C. Gerdes, "Modeling and control of an exhaust recompression HCCI engine using split injection," *J. Dyn. Syst. Meas. Control*, vol. 134, no. 1, pp. 011016-1–011016-12, Jan. 2012.
[28] C. Marriott and R. Reitz, "Experimental investigation of direct injection-gasoline for premixed compression ignited combustion phasing control," General Motors Powertrain, Univ. Wisconsin-Madison, Madison, WI, USA, Tech. Rep. 2002-01-0418, 2002.
[29] J.-O. Olsson, P. Tunestål, and B. Johansson, "Closed-loop control of an HCCI engine," *SAE Trans.*, vol. 110, no. 3, pp. 1076–1085, 2001.
[30] J. Bengtsson, P. Strandh, R. Johansson, P. Tunestål, and B. Johansson, "Hybrid modelling of homogeneous charge compression ignition (HCCI) engine dynamic-a survey," *Int. J. Control*, vol. 80, no. 11, pp. 1814–1848, Nov. 2007.
[31] J. Heywood, *Internal Combustion Engine Fundamentals*. New York, NY, USA: McGraw-Hill, 1988.
[32] S. Jade, E. Hellström, A. Stefanopoulou, and L. Jiang, "On the influence of composition on the thermally-dominant recompression HCCI combustion dynamics," in *Proc. ASME Dyn. Syst. Contr. Conf.*, 2011, pp. 1–8.
[33] N. Ravi, N. Chaturvedi, J. Oudart, D. Cook, E. Doran, A. Kojic, *et al.*, "Control-oriented physics-based modeling of engine speed effects in HCCI," in *Proc. IEEE Conf. Decision Control*, Dec. 2012, pp. 4947–4952.
[34] E. Hellström and A. G. Stefanopoulou, "Modeling cyclic dispersion in autoignition combustion," in *Proc. 50th IEEE CDC-ECC*, Dec. 2011, pp. 6834–6839.
[35] S. R. Turns, *An Introduction to Combustion: Concepts and Applications*, 2nd ed. New York, NY, USA: McGraw-Hill, 2000.
[36] J. Livengood and P. Wu, "Correlation of autoignition phenomena in internal combustion engines and rapid compression machines," in *Proc. Symp. Int. Combust.*, vol. 5. 1955, pp. 347–356.
[37] J. Larimore, E. Hellström, S. Jade, L. Jiang, and A. G. Stefanopoulou, "Controlling combustion phasing variability with fuel injection timing in a multicylinder HCCI engine," in *Proc. Amer. Control Conf.*, Jun. 2013, pp. 4435–4440.
[38] B. Allison and A. Isaksson, "Design and performance of mid-ranging controllers," *J. Process Control*, vol. 8, nos. 5–6, pp. 469–474, 1998.
[39] M. Karlsson, K. Ekholm, P. Strandh, R. Johansson, P. Tunestål, and B. Johansson, "Closed-loop control of combustion phasing in an HCCI engine using VVA and variable EGR," in *Proc. 5th IFAC Symp. Adv. Autom. Control*, 2007, pp. 501–508.
[40] N. Ravi, H.-H. Liao, A. F. Jungkunz, and J. C. Gerdes, "Mid-ranging control of a multi-cylinder HCCI engine using split fuel injection and valve timings," in *Proc. 6th IFAC Symp. Adv. Autom. Control*, 2010, pp. 797–802.
[41] E. G. Gilbert and I. Kolmanovsky, "Fast reference governors for systems with state and control constraints and disturbance inputs," *Int. J. Robust Nonlinear Control*, vol. 9, pp. 1117–1141, Jun. 1999.
[42] C. Chiang and A. G. Stefanopoulou, "Stability analysis in homogeneous charge compression ignition (HCCI) engines with high dilution," *IEEE Trans. Control Syst. Technol.*, vol. 15, no. 2, pp. 209–219, Mar. 2007.
[43] H.-H. Liao, N. Ravi, A. Jungkunz, A. Widd, and J. C. Gerdes, "Controlling combustion phasing of recompression HCCI with a switching controller," in *Proc. 6th IFAC Symp. Adv. Autom. Control*, 2010, pp. 821–826.

Shyam Jade (S'11) received the bachelor's degree from the Indian Institute of Technology, Bombay, India, and the master's degree from the University of Michigan, Ann Arbor, MI, USA, in 2009 and 2011, respectively, both in mechanical engineering, where he is currently pursuing the Ph.D. degree in mechanical engineering.

His current research interests include modeling and control systems development for advanced internal combustion engines.

Erik Hellström (M'11) received the M.Sc. degree in applied physics and electrical engineering and the Ph.D. degree from Linköping University, Linköping, Sweden, in 2005 and 2010, respectively.

He is currently an Assistant Research Scientist with the Department of Mechanical Engineering, University of Michigan, Ann Arbor, MI, USA. His current research interests include modeling, control, and optimal control of vehicle power trains.

Jacob Larimore (S'11) received the bachelor's degree from the Missouri University of Science and Technology, Rolla, MO, USA, and the master's degree from the University of Michigan, Ann Arbor, MI, USA, in 2009 and 2012, respectively, both in mechanical engineering, where he is currently pursuing the Ph.D. in mechanical engineering.

His current research interests include modeling and control of advanced internal combustion engines and embedded control systems.

Anna G. Stefanopoulou (S'93–M'96–SM'05–F'09) is a Professor of mechanical engineering with the University of Michigan, Ann Arbor, MI, USA, and the Director of the Automotive Research Center, a university-based U.S. Army Center of Excellence in Modeling and Simulation of Ground Vehicles. She was an Assistant Professor with the University of California, Santa Barbara, CA, USA, from 1998 to 2000, and a Technical Specialist with Ford Motor Company, Dearborn, MI, USA, from 1996 to 1997. She has co-authored a book *Control of Fuel Cell Power Systems*, holds ten U.S. patents, and 200 publications on estimation and control of internal combustion engines and electrochemical processes such as fuel cells and batteries.

Prof. Stefanopoulou received five Best Paper Awards. She is an ASME, the Inaugural Chair of the ASME DSCD Energy Systems Technical Committee, and a member of the SAE Dynamic System Modeling Standards Committee and the U.S. National Academies committee on Vehicle Fuel Economy Standards.

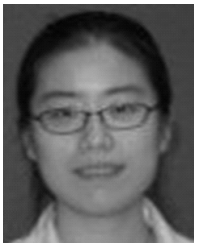

Li Jiang received the bachelor's degree in mechanical engineering from Shanghai Jiao Tong University, Shanghai, China, and the master's degree in electrical engineering system and the Ph.D. degree in mechanical engineering from the University of Michigan, Ann Arbor, MI, USA.

She is a Senior System Engineer, leading control system development for engine management system applications, with System and Advanced Engineering at Robert Bosch LLC, Farmington Hills, MI, USA, Gasoline Systems North America. She is the Co-Principal Investigator of Bosch and the U.S. Department of Energy joint research projects on Advanced Combustion Concepts-Enabling Systems and Solutions and the recently awarded Recirculated Exhaust Gas Intake Sensing.